Heat of Fusion and Surface Tension of Solids Confined in Porous Materials Derived from a Combined Use of NMR and Calorimetry

ARTICLE *in* THE JOURNAL OF PHYSICAL CHEMISTRY B · AUGUST 1997

Impact Factor: 3.3 · DOI: 10.1021/jp9710594

3 AUTHORS, INCLUDING:

Eddy Walther. Hansen
University of Oslo
112 PUBLICATIONS **1,475** CITATIONS

SEE PROFILE

Heat of Fusion and Surface Tension of Solids Confined in Porous Materials Derived from a Combined Use of NMR and Calorimetry

E. W. Hansen,*,† H. C. Gran,‡ and E. J. Sellevold§

SINTEF Applied Chemistry, P.O. Box 124, Blindern, 0314 Oslo, Norway, Norwegian Building Research Institute, P.O. Box 123, Blindern, 0314 Oslo, Norway, Department of Chemistry, University of Oslo, P.O. Box 1033, Blindern, 0315 Oslo, Norway, and Department of Structural Engineering, NTNU, 3034 Trondhein, Norway

Received: March 25, 1997; In Final Form: May 28, 1997⊗

Assuming the heat of fusion (Δh_f) of a material confined in a porous material to be approximated by a function $\Delta h_f = \Delta h_0\,(1 + a_0(10^3/T) + a_1(10^3/T)^2)$, where T is the absolute temperature, a theoretical model is derived that enables the coefficients a_i to be determined from a combined use of NMR and calorimetric measurements. The model has been applied on solid ice confined in cement pastes resulting in $a_0 = -0.136$ K and $a_1 = -0.00413$ K^2 in the temperature range 273 K > T > 210 K. Δh_0 was determined from the known value of Δh_f of bulk water at 273 K, giving $\Delta h_0 = 749$ J/g. Likewise, assuming the surface tension (γ) of the ice−water interface to be approximated by a corresponding second-order polynomial in $1/T$, i.e., $\gamma = \gamma_0\,(1 + b_0(10^3/T) + b_1(10^3/T)^2)$, the coefficients b_i were determined from the Gibbs−Thomson equation: $\Delta T = K_f(\gamma/\rho\Delta h_f)(1/R)$, where K_f is a constant, ρ the density, and ΔT the lowering of the melting point of ice confined in pores with radius R. The model fit revealed a best fit to a linear function in $1/T$, with $b_1 = 0$ and $b_0 = -(0.114 \pm 0.033)$ *K*. The γ_0 was determined from the known value of γ at 273 K, resulting in $\gamma_0 = 130$ erg/cm.

Introduction

There is a general interest in the behavior of liquids and solids in porous materials at temperatures below bulk freezing temperature. The topic has importance in several areas covering soil,[1,2] biological systems,[3,4] and building materials.[5−8] Various techniques have been used to study frost mechanisms, NMR,[1,8−11] measurement of internal friction and elastic modulus,[12,13] measurement of dimensional changes,[14−16] low-temperature calorimetry, and DSC,[6,17] as well as pore structure characterization[18,19] in different materials. Investigations on the characterization of pore structure include mesoporous materials,[19−22] controlled pore glasses, activated charcoal, and silica gel[23] with well-characterized pore structures and usually uniform pore sizes. These studies have been carried out with both water and different organic liquids occupying the pore structure. Studies of frost mechanisms performed on soil[1,2] and biological systems[3,4] and building materials as hardened cement/concrete[5−8] may serve as examples.

An important parameter connected to solid−liquid phase transitions is the heat of fusion, Δh_f, of the pore liquid. Studies dealing with the heat of fusion of solids confined in porous systems are however rare. Radjy and Sellevold[13] calculated the amounts of ice formed with low-temperature calorimetry using enthalpy data for water and ice derived from extrapolations of literature values of vapor pressure for ice and water. The heat of fusion increased with temperature according to the equation $\Delta h_f = 79.7 + 0.54$ T (°C) cal/g. The values for the heat of fusion as a function of temperature agreed well with values given by Defay et al.[24] down to −20 °C. Strange and co-workers[18] described a pore characterization technique combining NMR intensity data and freezing point depression based on the Gibbs−Thompson equation assuming Δh_f to be constant and equal to the bulk value.

The Gibbs−Thompson equation predicts a linear correlation between $1/R$ and the freezing point depression, ΔT. A linear relationship has been observed in the literature by Rennie and Clifford[25] and Jackson and McKenna.[26] Hansen and Gran[8] found on the other hand a nonlinear correlation between $1/R$ and ΔT from comparison of NMR and mercury porosimetry data. The nonlinearity was assumed to be a consequence of variations in Δh_f and/or surface tension with temperature.

The relationship between Δh_f and $1/R$ is not well understood. Contradictory results are reported in the literature, and both reduction, Litvan,[14] and increase, Patric and Kemper,[27] are reported. Jackson and McKenna measured phase transition temperatures and heats of fusion of nonpolar organic solids confined in pores of controlled pore glasses. They found a rapid decrease of Δh_f for pore radii smaller than 250−300 Å and mentioned the contact angle between the liquid, solid, and the pore wall as one possible factor explaining the behavior. They also draw attention to cluster theory where the melting point depression in Lennard-Jones clusters for very small radii predicts that $\Delta T \propto 1/R^2$ rather than that $\Delta T \propto 1/R$.

In this work, the process of melting of water confined in a pore system is studied by a combination of ^{1}H-NMR and low-temperature calorimetry. The amount of ice melted as measured by NMR is correlated to the amount of heat released from the ice as measured by low-temperature calorimetry. The NMR and calorimetry data are approximated by second-order polynomials to determine the heat of fusion (Δh_f) and surface tension (γ) as a function of temperature at subzero temperatures.

Experimental Section

Materials. NMR and freeze calorimetry measurements were performed on samples prepared from two different hydrated cement pastes, A and B. The cement pastes differed only in the mix ratio between water and dry cement powder, paste A

* To whom correspondence should be addressed.
† SINTEF Applied Chemistry.
‡ Norwegian Building Research Institute/University of Oslo.
§ NTNU.
⊗ Abstract published in *Advance ACS Abstracts,* July 1, 1997.

S1089-5647(97)01059-6 CCC: $14.00

having a water/cement ratio of 0.40 and paste B having a water/cement ratio of 0.60. Sample B exhibits a large amount of capillary pores created by a surplus of mix water in relation to cement powder, while the pore system in sample A is mainly of mesoporous character. Both hydrated cement pastes were cast 3 months prior to the start of the experiments. Cement pastes for freeze calorimetry were produced and tested at an earlier date. The composition of the cements was therefore different. The cement pastes used for freeze calorimetry were produced from a Danish Super White Portland Cement with a Bogue composition of 88.4% tricalcium silicate (C_3S), 2.4% dicalcium silicate (C_2S), 5.04% tricalcium aluminate (C_3A), and 0.94% tetracalcium alumina ferrite (C_4AF). The cement pastes used for NMR measurements were made from a Danish Super White Portland with a Bogue composition of 75% tricalcium silicate (C_3S), 15% dicalcium silicate (C_2S), 4% tricalcium aluminate (C_3A), and 1% tetracalcium alumina ferrite (C_4AF), certified as a British Standards Institution class 62.5N cement. Both cements were manufactured by Aalborg Portland. The reason for using a white cement was its low content of paramagnetic constituents as Fe_2O_3 and Mn_2O_3 that may contribute to NMR relaxation.[28] All pastes were mixed carefully under a slight vacuum and vibrated to avoid entrapped air voids and molded in sealed polytetrafluoroethane forms with diameter 20 mm and length 120 mm. Both pastes were rotated slowly during the first 20 h of hardening to avoid separation between water and cement. The pastes were stored in water at room temperature after demolding.

Two samples of cylindrical shape were cut from each of the two pastes, one sample to be used for the freeze calorimetry measurements (samples from now on denoted C04 and C06 with w/c = 0.40 and 0.60, respectively) and the other sample to be used for the NMR measurements (samples from now on denoted S04 and S06 with w/c = 0.40 and 0.60, respectively). The two freeze calorimetry samples were cut to a length of 60 mm and a diameter of 14.6 mm, while the smaller NMR samples had a length of 10 mm and diameter of 3.5 mm.

The cement pastes were tested for evaporable water content by measuring the weight loss when heating virgin (never dried) samples from an initial saturated surface dry (SSD) condition at 105 °C until constant weight. The evaporable water content was measured to 18.8% by weight of sample (SSD) for w/c ratio 0.40 and 32.6% by weight of sample (SSD) for w/c ratio 0.60. Weight of samples were $m_{S04} = 0.1981$ g, $m_{S06} = 0.1959$ g, $m_{C04} = 14.549$ g, and $m_{C06} = 14.508$ g.

Low-Temperature Calorimetry. The experiments were carried out on a SETARAM Low Temperature Calvet Micro calorimeter using a differential scanning mode of operation. Data were recorded in the temperature range from −60 to 10 °C. Samples were heated at a rate of 3.3 °C/h. The temperature recorded during an experiment and used in data presentations is that of the calorimeter block. Measured drift in the system never exceeded 0.5% of the output represented by a typical hydrated cement paste specimen. Control experiments were run with pure water. The mean Δh determined from heating and cooling of water in a slit and a gap was 333.8 J/g compared to the correct value of 333.3 J/g.

The amount of heat released during melting was calculated according to a description given by de Fontenay and Sellevold,[6] while some of the results utilized here are given by Sellevold et al.[29]

NMR. The intensity of the water signal vs temperature (in the range −100 °C to room temperature) was followed by ^{1}H-NMR. The accuracy of the temperature determination was within ±0.5 °C. A Varian VXR 300 S NMR spectrometer, operating at 300 MHz proton resonance frequency, was used with a bandwidth of 100 kHz and an acquisition time of 0.125 s. Each spectrum was composed of 16 transients. The pulse length was set to 20 μs, corresponding to a pulse angle of 90°. Due to the short spin−lattice relaxation times, a pulse repetition time of 3 s was sufficient. Each sample was initially cooled down to 173 K and then heated in steps of 1 K after being temperature equilibrated for 2 min at each new temperature setting before initiating the NMR acquisition experiment. The intensity (integral) of the mobile water was corrected for temperature (Curie's law) and monitored vs temperature (*IT* curve).

Theoretical Model

Hansen and co-workers[19−22] have previously derived a model relating the ^{1}H-NMR signal intensity of residual water (I) confined in a porous material vs temperature T:

$$I(T) = \frac{1}{\sqrt{\pi}} I_0 \int_{-\infty}^{(1/T-1/T_c)/\sqrt{2}\sigma} \exp(-u^2)\, du \qquad (1)$$

where T_c represents a critical inverse temperature equivalent to the melting point of ice within the porous material. The parameter σ defines the width of the melting point distribution curve, which approaches zero for a porous material composed of a single and unique pore dimension R. I_0 represents the NMR signal of the confined water when all ice is melted. In general, the melting point, T_c, will be related to the pore dimension via the Gibbs−Thomson equation:[30,31]

$$T_0 - T = \Delta T = K_f \frac{\gamma}{\rho \Delta h_f} \frac{1}{R} \qquad (2)$$

where T_0 is the melting point of bulk ice, K_f is a constant, ρ is the density of water, Δh_f is the heat of fusion, and γ is the solid−liquid surface tension. If the porous material is characterized by a distribution of pore sizes about a mean value R, this will be reflected by a corresponding distribution in melting points as already stated by the width parameter σ in eq 1.

If the pore size distribution is nonuniform, it can always be approximated by a discrete number of pore size distributions of widths σ_{R_i} about the mean values R_i. This implies that the corresponding NMR signal intensity of the water signal vs temperature can be expressed by a generalized form of eq 1:

$$I(T) = \frac{1}{\sqrt{\pi}} \sum_i I_{0i} \int_{-\infty}^{(1/T-1/T_{ci})/\sqrt{2}\sigma_i} \exp(-u^2)\, du \qquad (3)$$

It is known that the enthalpy of melting (Δh_f) is a function of temperature,[6,16,24,28,32] implying that it can always be approximated by a polynomial function in $1/T$:

$$\Delta h_f = \sum_i c_i (10^3/T)^i \qquad (4)$$

where c_i are constants. The heat (δQ) released when an infinitesimal amount (dm) of ice melts can thus be written $\delta Q = \Delta h_f\, dm$, where the symbol δ is used to denote an infinitesimal change in Q rather than dQ, since Q is not a state function of the system but depends on the path of the process. Since the NMR signal intensity (I) is directly proportional to the amount of water, we can write $dI = k\, dm$, where k is a constant. Combining these equations and differentiating with respect to $1/T$, the following equation is obtained when substituting eq 3 for $I(T)$:

$$\frac{\delta Q}{\mathrm{d}(1/T)} = k\Delta h_f(T)\frac{\mathrm{d}I}{\mathrm{d}(1/T)} = \frac{k}{\sqrt{2\pi}}\sum_{i=1}\frac{I_{0i}}{\sigma_i}\Delta h_f(T)\exp\left(-\left(\frac{1/T - 1/T_{ci}}{\sqrt{2}\sigma_i}\right)^2\right) \quad (5)$$

The coefficients a_i of eq 4, and thus the temperature dependence of Δh_f, can be derived by fitting eq 5 to the observed $\delta Q/\mathrm{d}(1/T)$ data by a nonlinear least squares fit. However, we have noticed that a better way to analyze the data is by fitting the observed cumulative heat (Q) released during warming of the sample from low temperature ($T \approx 0$) to a specific temperature T, corresponding to the integrated form of eq 5, i.e.,

$$Q(T) = -\frac{k}{\sqrt{2\pi}}\sum_{i=1}\frac{I_{0i}}{\sigma_i}\int_{1/T}^{\infty}\Delta h_f(u)\exp\left(-\left(\frac{u - 1/T_{ci}}{\sqrt{2}\sigma_i}\right)^2\right)\mathrm{d}u \quad (6)$$

Approximating Δh_f by a second-order polynomial in $1/T$, eq 7,

$$\Delta h_f(T) = \Delta h_0(1 + a_0(10^3/T) + a_1(10^3/T)^2) \quad (7)$$

results in the following "analytical" solution of the cumulative heat of fusion:

$$Q = k\sum_{i=1}\left(A_{0i}\left(1 - \mathrm{erf}\left(\frac{1/T - 1/T_{ci}}{\sqrt{2}\sigma_i}\right)\right) + \left[A_{1i} + A_{2i}\frac{1/T - 1/T_{ci}}{\sqrt{2}\sigma_i}\right]\exp\left[-\left(\frac{1/T - 1/T_{ci}}{\sqrt{2}\sigma_i}\right)^2\right]\right) \quad (8a)$$

where k is a constant and the coefficients A_i are given by

$$A_{0i} = \frac{1}{2}I_{0i}\Delta h_0[1 + a_0(1/T_{ci}) + a_1(1/T_{ci})^2 + \sigma_i^2 a_1] \quad (8b)$$

$$A_{1i} = \frac{1}{\sqrt{2\pi}}I_{0i}\Delta h_0[a_0\sigma_i + 2a_0\sigma_i(1/T_{ci})] \quad (8c)$$

$$A_{1i} = \frac{1}{\sqrt{\pi}}I_{0i}\Delta h_0 a_1\sigma_i^2 \quad (8d)$$

The function "erf" is defined by $\mathrm{erf}(Y) = (2/\sqrt{\pi})\int_0^y \exp(-U^2)\,\mathrm{d}U$. The details concerning the derivation of these integrals are shown in the Appendix. Note that if the enthalpy of fusion is independent of temperature ($a_0 = a_1 = 0$), the cumulative heat of fusion (Q) will have the same shape as the NMR *IT* curve, i.e., $Q = kI(T)$.

Results and Discussion

The NMR *IT* curves of cement pastes with different water/cement (w/c) ratios have previously been reported.[8] Two of these *IT* curves are reproduced in Figure 1 and correspond to samples S04 and S06, respectively. The solid curves represent model fits to eq 3. The fitted parameters are tabulated in Table 1. The corresponding cumulative heats of fusion of sample C04 and C06 are shown in Figure 2a,b. The solid curve in Figure 2a represents a nonlinear least squares model fit of eq 8 to the observed data resulting in $a_0 = -0.115$ K and $a_1 = -0.005\,75$ K^2. The parameter Δh_0 was determined by the known value of Δh_f (333.5 J/g) at $T = 273$ K and gives $\Delta h_0 = 661$ J/g. The derived temperature dependence of the heat of fusion (Δh_f) is plotted in Figure 3 (black dots) together with data calculated by Radjy[12,13] and Helmuth[33] from extrapolations of tabulated values[34] of vapor pressure for ice and water (solid curve). These latter Δh_f values agree to within about 1% down to 253 K with values given by Defay et al.[24] The Δh_f values obtained by the combined use of NMR and calorimetry are systematically larger by less than 10% in the temperature range 210 K < T < 273 K. In order to obtain an improved and more reliable estimate of the heat of fusion, the cumulative heat of fusion of a second cement paste, sample C06 was used. Equation 8 was fitted to the two cumulative heat of fusion curves (Q_{C04} and Q_{C06} in Figure 2b) simultaneously by assuming the same second-order polynomial approximation of Δh_f for the two samples (eq 7). The model fits are shown by the solid/dotted curves in Figure 2b with $a_0 = -0.136$ K, $a_1 = -0.004\,13$ K^2, and $\Delta h_0 = 749$ J/g. The latter parameter was determined from the known bulk value of the heat of fusion at 273 K. This temperature dependent heat of fusion is shown by the open-dot curve in Figure 3 and deviates by less than 4% from the previously reported literature values (solid curve in Figure 3) in the temperature range 210 K < T < 273 K. A decrease in the heat of melting vs decreasing temperature has been reported previously by Jackson et al.[26] for a number of organic materials confined in porous solids.

Hansen and Gran[8] have recently presented data that relate pore dimension (R) obtained by mercury intrusion porosimetry (MIP) to melting point depression (ΔT) of confined water obtained by NMR on four different cement pastes with w/c = 0.4, 0.6, 0.7, and 1.0. These data are reproduced in Figure 4 and enable the temperature dependence of the surface tension of water confined in the cement pastes to be obtained from the Gibbs−Thomson equation (eq 2). Assuming the density of

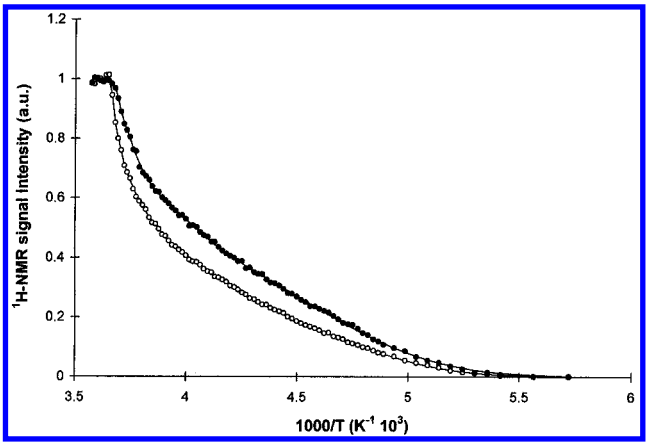

Figure 1. ^{1}HNMR signal intensity vs inverse temperature (I/T curve) of samples S04 (●) and S06 (○) during heating of the samples from 173 to 280 K. The solid curves represent model fits by eq 1.

TABLE 1: Numerical Values of Transition-Temperature/Melting-Temperature T_{ci}, the Width of the Melting Point Distribution, σ_i, and Intensity of the Transition, I_i, Obtained by Fitting Eq 3 to the Observed *IT* Curves of Samples S04 and S06: The Intensity Has Been Normalized, i.e., $\sum I_i = 1$

	sample	
parameter	S04	S06
I_1	0.275 ± 0.040	0.208 ± 0.032
σ_1 (K^{-1})	0.051 ± 0.006	0.020 ± 0.003
$X_{c1} = 1000/T_{c1}$ (K^{-1})	3.736 ± 0.002	3.685 ± 0.002
I_2	0.286 ± 0.082	0.177 ± 0.046
σ_2 (K^{-1})	0.198 ± 0.041	0.080 ± 0.019
$X_{c2} = 1000/T_{c2}$ (K^{-1})	3.944 ± 0.042	3.795 ± 0.023
I_3	0.439 ± 0.039	0.615 ± 0.061
σ_3 (K^{-1})	0.415 ± 0.028	0.627 ± 0.039
$X_{c3} = 1000/T_{c3}$ (K^{-1})	4.611 ± 0.048	4.102 ± 0.079

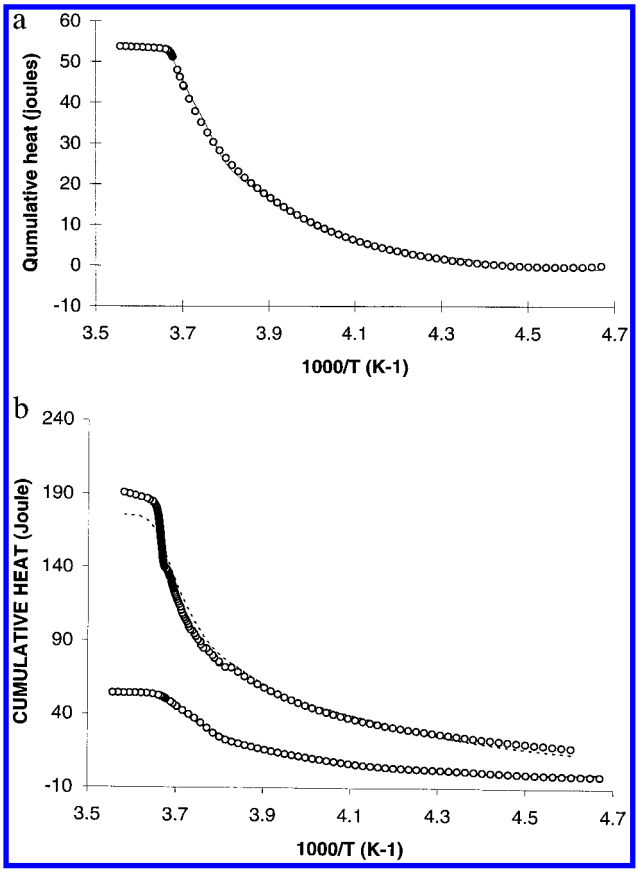

Figure 2. (a) Cumulative heat production (Q) vs inverse temperature X (=1000/T) as obtained by calorimetric measurements on sample C04. The solid curve represents a model fit by eq 8. (2) Cumulative heat production vs temperature as obtained by calorimetric measurements on samples C04 and C06. The solid and dotted curves represent a simultaneous model fit by eq 8 to the two cumulative heat production curves of samples C04 and C06, when assuming the temperature dependence of the heat of fusion to be identical for the two samples.

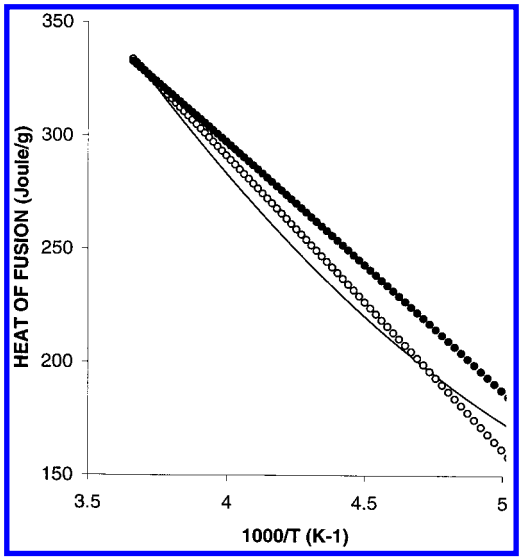

Figure 3. Enthalpy of melting (ΔH) vs inverse absolute temperature X (=1000/T) as derived from a combined use of NMR and calorimetry. The solid curve is based on literature data.[14] The data derived from sample A are shown by (●) and the data obtained by a combined use of samples A and B are shown by (○). See text for further details.

water (ρ) to be approximately constant and independent of temperature, only the surface tension (γ) remains undetermined. Using the same arguments as for the heat of fusion, i.e., approximating the temperature dependence of the surface tension by a second-order polynomial in 1/T,

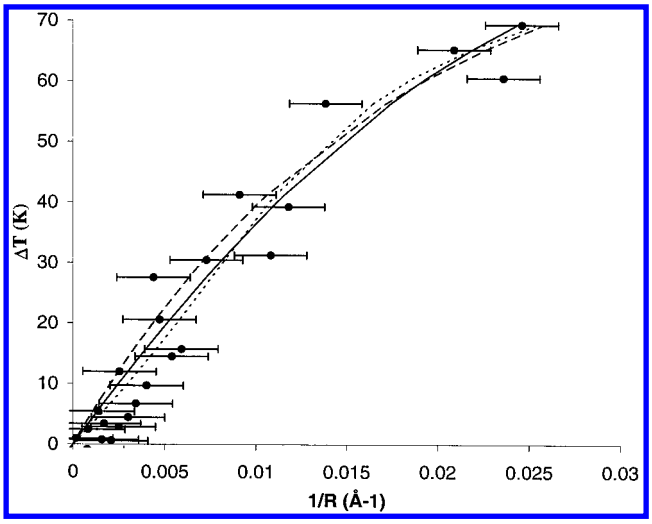

Figure 4. Melting point depression (ΔT) vs inverse pore dimension (1/R) obtained from a combined use of mercury intrusion porosimetry (MIP) and NMR.[8] The different curves represent model fits to eq 2 in combination with eqs 7 and 9 where (- - -) represents the temperature independent surface tension (γ), (—) represents a linear dependence of γ vs 1/T, and (···) represents a second-order temperature dependence of γ vs 1/T. See text for further details.

$$\gamma(T) = \gamma_0[1 + b_0(1/T) + b_1(1/T)^2] \qquad (9)$$

The data in Figure 4 have been fitted to eq 2 by inserting eq 7 for the temperature dependence of the heat of fusion and replacing the polynomial equation for the surface tension (eq 9). The three curves in Figure 4 represent model fits to eq 2 assuming a temperature independent surface tension (- - -, F = 125), a linear dependence of the surface tension vs 1/T (—, F = 304), and a second-order temperature dependence of the surface tension vs 1/T (···, F = 150). F is a statistical decision parameter. A larger F factor signifies a better fit and thus a "better" model description. Thus, the linear model gives the best fit to the observed data with $b_0 = -(0.114 \pm 0.033)$ K (and $b_1 = 0$). The value of γ_0 was estimated from the known value of γ (=75.6 erg/cm) at T = 273 K for water in contact with air, which gives γ_0 = 130 erg/cm. This value of γ (T = 273 K) is necessarily an approximation because the water is not in contact with air but with solid ice. The model fits predict a lowering of the surface tension with decreasing temperature, which has been reported by Clifford et al. back in 1976[25] on water confined in controlled-pore glasses having pore diameters in the range 70−2000 Å. Clifford et al. have used the same approach as described in this work, i.e., applying the Gibbs−Thomson equation to their ΔT vs 1/R data and correcting for the temperature (273 −250 K) of the other parameters in eq 2. A reference to how they have corrected the density or heat of fusion for temperature is not explicitly described and makes their temperature-derived surface tension somewhat dubious. When plotting their reported surface tensions against temperature and fitting it to a linear function in 1/T, a decrease in surface tension of approximately 40 ± 18% from 273 to 250 K is obtained, compared to only 7% obtained in this work. This difference is probably not significant when keeping in mind the large uncertainty estimated in surface tension from their reported data.

It should be emphasized, however, that the actual parameter determined in this work is the ratio γ/ρ rather than γ itself. Equation 9 is therefore valid only under the assumption that the density of water remains constant and independent of temperature. This assumption is somewhat disputable when considering water confined in very small pores, since the density

is conceptually a bulk parameter. Also, the increase in volume upon freezing of water will reduce the volume of any remaining nonfreezing water coexisting with solid ice, which might lead to a relative change in density of the remaining nonfreezing mobile water.

Another point of importance is that the Gibbs−Thomson equation, as represented by eq 2, is derived from a thermodynamic concept that relies on a large (infinite) number of particles or water molecules. This concept may break down for the limited number of water molecules confined in small pores (micro-mesopores). For smaller pore dimensions it might be necessary to introduce higher order terms $(1/R)^n$ in eq 2. For instance, computer simulations indicate that the melting transition of Lennard-Jones microcrystals confined to spherical cavities can be expressed by

$$\Delta T = A(1/R) - B(1/R)^2 \tag{10}$$

where A and B are constants.[26] This suggests that the curvature observed in Figure 4 can be rationalized by introducing such an additional, higher order pore dimension term $(1/R)^2$ in eq 2.[8] The exact reason for the observed curvature of ΔT vs inverse pore dimension (Figure 4) is thus somewhat ambiguous and disputable. Additional experimental and theoretical work is necessary to clarify these subtle but basic questions.

Conclusion

The combined use of NMR spectroscopy and calorimetry has been shown to represent an excellent tool for probing the temperature behavior of the heat of fusion of ice at subzero temperatures. The theoretical model used to obtain these data is rather general and can—in principle—be used to derive the temperature dependent heat of fusion of any material of interest. In practice, the technique is limited to solids having a melting temperature in the range 100−500 K. Moreover, applying the well-known Gibbs−Thomson equation enables the temperature dependence of the surface tension to be approximated, as well.

Appendix

Approximating the heat of fusion ΔH by a second-order polynomial vs the inverse absolute temperature u (=1000/T) in eq 6, the following formula for the cumulative heat (Q) vs inverse temperature (X) arises:

$$Q(X) = -\frac{k}{\sqrt{2\pi}}\sum_{i=1}\frac{I_{0i}}{\sigma_i}\int_{\infty}^{X}\Delta h_0(1 + a_0u + a_1u^2)\exp\left(-\left(\frac{u - X_{ci}}{\sqrt{2}\sigma}\right)^2\right)\mathrm{d}u \tag{A1}$$

The integration limits are determined by the experimental conditions, i.e., the heat produced when heating the sample from low temperature ($T \approx 0 \Rightarrow u = 1000/T \approx \infty$) to a finite inverse temperature u (=1000/T). Introducing a new variable $z = (u - X_{ci})/\sqrt{2}\sigma_i$, eq A1 can be transformed to

$$Q(X) = \frac{k\Delta h_0}{\sqrt{2\pi}}\sum_{i=1}\frac{I_{0i}}{\sigma_i}\int_{(X-X_{ci})/\sqrt{2}\sigma_i}^{\infty}(1 + a_0(X_{ci} + \sqrt{2}\sigma_i z) + a_1(X_{ci} + \sqrt{2}\sigma_i z)^2)\exp(-z^2)\,\mathrm{d}z \tag{A2}$$

Upon rearrangement of eq A2, the integral terms $\int z\exp(-z^2)\,\mathrm{d}z$ and $\int z^2\exp(-z^2)\,\mathrm{d}z$ arise, which can be easily solved by partial integration, i.e.,

$$\int z\exp(-z^2)\,\mathrm{d}z = -\frac{1}{2}\exp(-z^2)$$

and

$$\int z^2\exp(-z^2)\,\mathrm{d}z = -\frac{1}{2}z\exp(-z^2) + \frac{1}{2}\int\exp(-z^2)\,\mathrm{d}z$$

Introducing these expressions into eq A2 and performing some simple but tedious algebra, eq 8 appears.

A few remarks when applying the error function, defined by $\mathrm{erf}(Y) = (2/\sqrt{\pi})\int_0^Y\exp(-U^2)\,\mathrm{d}U$ to calculate the integral $\int_a^{\infty}\exp(-z^2)\,\mathrm{d}z$ are necessary since the integration limit a can attain both negative and positive values. Since the error function is normally tabulated for positive Y, we can always express this latter integral as

$$\int_a^{\infty}\exp(-z^2)\,\mathrm{d}z = \int_0^{\infty}\exp(-z^2)\,\mathrm{d}z - \int_0^{a}\exp(-z^2)\,\mathrm{d}z \tag{A3}$$

where

$$\int_a^{\infty}\exp(-z^2)\,\mathrm{d}z = \frac{\sqrt{\pi}}{2}(\mathrm{erf}(\infty) + \mathrm{erf}(\mathrm{abs}(a))) \quad \text{for negative } a$$

and

$$\int_a^{\infty}\exp(-z^2)\,\mathrm{d}z = \frac{\sqrt{\pi}}{2}(\mathrm{erf}(\infty) + \mathrm{erf}(\mathrm{abs}(a))) \quad \text{for positive } a$$

implying that

$$\int_a^{\infty}\exp(-z^2)\,\mathrm{d}z = \frac{\sqrt{\pi}}{2}\left(\mathrm{erf}(\infty) - \frac{a}{\mathrm{abs}(a)}\mathrm{erf}(\mathrm{abs}(a))\right) \tag{A4}$$

irrespective of the sign of a. Equation A4 has thus been used throughout in this work when calculating the integral $\int_a^{\infty}\exp(-z^2)\,\mathrm{d}z$.

References and Notes

(1) Tice, A. R.; Oliphant, J. L.; Nakano, Y.; Jenkins, T. F. Cold Regions Research Laboratory, CRREL Report 82−15; 1982; p 15.
(2) Tice, A. R.; Anderson, D. M.; Sterrett, K. F. *Eng. Geol.* **1981**, *18*, 135−146.
(3) Murase, N.; Gonda, K.; Watanabe, T. *J. Phys. Chem.* **1986**, *90*, 5420
(4) Katayama, S.; Fujiwara, S. *J. Phys. Chem.* **1980**, *84*, 2320−2325.
(5) Powers, T. C., Brownyard, T. L. Res. Labs. Portland Cement Association Bulletin 22; March 1948.
(6) le Sage de Fontenay, C.; Sellevold, E. J. Durability of Building Materials and Components, ASTM STP 691; 1980; p 425.
(7) Bager, D. H.; Sellevold, E. J. *Cem. Concr. Res.* **1986**, *16*, 709.
(8) Hansen, E. W.; Gran, H. C. Submitted for publication.
(9) Pearson, R. T.; Derbyshire, W. J. *Colloid Interface Sci.* **1974**, *46*, 232−248.
(10) Resing, H. A.; Thompson, J. K.; Krebs, J. J. *J. Phys. Chem.* **1964**, *7*, 1621.
(11) Resing, H. A. *J. Phys. Chem.* **1965**, *43*, 669.
(12) Sellevold, E. J.; Radjy, F. J. *Mater. Sci.* **1976**, *11*, 1927.
(13) Radjy, F.; Sellevold, E. J. *Nature* **1973**, *241* (111), 133−135.
(14) Litvan, G. G. *Can. J. Chem.* **1966**, *44*, 2617.
(15) Litvan, G. G. J. *Colloid Interface Sci.* **1973**, *45* (1), 154−169.
(16) Litvan, G. G. *Cem. Concr. Res.* **1976**, *6*, 351−356.
(17) Dorner, H. W. *Cem. Concr. Res.* **1984**, *14*, 807−815.
(18) Strange, J. H.; Rahman, M.; Smith, E. G. *Phys. Rev. Lett.* **1993**, *71* (21), 3589.
(19) Hansen, E. W.; Schmidt, R.; Stöcker, M. *J. Phys. Chem.* **1996**, *100*, 11396.
(20) Hansen, E. W.; Stöcker, M.; Schmidt, R. *J. Phys. Chem.* **1996**, *100*, 2195−2200.
(21) Schmidt, R.; Hansen, E. W.; Stöcker, M.; Akporiaye, D.; Ellestad, O.-H. *J. Am. Chem. Soc.* **1995**, *117*, 4049−4056.
(22) Hansen, E. W.; Schmidt, R.; Stöcker, M.; Akporiaye, D. *J. Phys. Chem.* **1995**, *9*, 4148−4154.

(23) Overloop, K.; Van Gerven, L. *J. Magn. Reson. Ser. A* **1993**, *101*, 179.

(24) Defay, R.; Prigogine, I.; Bellemans, A.; Everett, D. H. *Surface Tension and Adsorption*; Wiley: New York, 1957; p 248.

(25) Rennie, G. K.; Clifford, J. *J. Chem. Soc., Faraday Trans 1* **1977**, *73*, 680−89.

(26) Jackson, C. L.; McKenna, G. B. *J. Phys. Chem.* **1990**, *93* (12), 9002.

(27) Patrick, W. A.; Kemper, W. A. *J. Phys. Chem.* **1938**, *42*, 369.

(28) Bhattacharja, S.; Moukawa, M.; D'Orazio, F.; Jehng, J.; Halperin, W. P. *Adv. Cem. Based Mater.* **1993**, *1*, 67−76.

(29) Sellevold, E. J.; Bager, D. H.; Klitgaard Jensen, E.; Knudsen, T. *Silica Fume-Cement Pastes: Hydration and Pore Structure*, Proceedings Nordic Mini Seminar Condensed Silica Fume in Concrete; Div. of Building Materials, NTH, Trondheim, Feb 1982, BML Report 82−610; 1982; pp 20−50.

(30) Gibbs, J. W. *Collected Works*; Longmans: Green, New York, 1928.

(31) Thompson, W. (Lord Kelvin) *Philos. Mag.* **1871**, *42*, 448.

(32) Morioka, Y.; Kobayashi, J.; Higuchi, I. *J. Colloid Interface Sci.* **1973**, *42*, 1, 156.

(33) Helmuth, R. A. National Bureau of Standards Monograph 43, Vol.2; Proceedings, 4th International Symposium on the Chemistry of Cement, Washington, DC, 1960.

(34) *Handbook of Chemistry and Physics*, 53rd ed.; Chemical Rubber Co.: Cleveland, OH, 1972.